Two-nodal surface phonons in solid-state materials

Chengwu Xie,[1,*] Hongkuan Yuan,[1,*] Ying Liu,[2,†] and Xiaotian Wang[1,‡]
[1]*School of Physical Science and Technology, Southwest University, Chongqing 400715, China*
[2]*School of Materials Science and Engineering, Hebei University of Technology, Tianjin 300130, China*

(Received 5 December 2021; revised 23 January 2022; accepted 28 January 2022; published 14 February 2022)

This year, researchers have been on the lookout for real materials with one-nodal, two-nodal (two-NS), and three-nodal surface phonons. However, materials with two-NS phonons have been scarce until recently. This paper contributes to the understanding of the symmetry conditions of two-NS phonons. Two-NS phonons have NS states that are localized on two of three $k_i = \pm\pi$ ($i = x, y, z$) planes in the three-dimensional Brillouin zone). They are dominated by twofold screw symmetry and time-reversal symmetry. This paper also contributes the prediction of a series of materials with two-NS states in their phonon dispersions. First, by screening all 230 space groups (SGs), we discovered 19 SG candidates (with Nos. 18, 55–60, 90, 94, 113, 114, 127–130, and 135–138) that have two-NS phonons. Second, based on first-principles calculations, we proposed 19 realistic material candidates hosting two-NS phonons: $P2_12_12$-type $ZnTeMoO_6$ (with SG No. 18), *Pbma*-type Cs_2Te_2 (with SG No. 55), *Pccn*-type Sr_2SnO_4 (with SG No. 56), *Pbcm*-type CaAlPd (with SG No. 57), *Pnnm*-type PtO_2 (with SG No. 58), *Pmmn*-type KLi_2As (with SG No. 59), *Pbcn*-type CV_2 (with SG No. 60), $P42_12$-type $BaVCu_4P_4O_{17}$ (with SG No. 90), $P4_22_12$-type $Na_5Fe_3F_{14}$ (with SG No. 94), $P\bar{4}2_1m$-type BaS_3 (with SG No. 113), $P\bar{4}2_1c$-type Na_4SnS_4 (with SG No. 114), $P4/mbm$-type ReO_3 (with SG No. 127), $P4/mnc$-type $Sr_4Li_2Si_4N_8O$ (with SG No. 128), $P4/nmm$-type $BaHfN_2$ (with SG No. 129), $P4/ncc$-type Bi_2CuO_4 (with SG No. 130), $P4_2/mbc$-type YB_2C (with SG No. 135), $P4_2/mnm$-type MgF_2 (with SG No. 136), $P4_2/nmc$-type YB_4Rh_4 (with SG No. 137), and $P4_2/ncm$-type $LiClO_2$ (with SG No. 138). Third, we discovered 622 (out of 10 037) materials with two-NS phonons by checking the phonon database at Kyoto University. Our present paper provides a better understanding of the two-NS states in phonon systems (or even other bosonic systems) and suggests a huge number of material candidates with two-NS phonons.

DOI: 10.1103/PhysRevB.105.054307

I. INTRODUCTION

Emergent particles in condensed-matter physics can have a wide range of types and physical properties [1,2]. For example, electron quasiparticles in solids can have various dispersion types and topological charges in addition to the elementary Weyl [3,4], Dirac [5,6], and Majorana [7,8] fermions, and their distribution in the momentum space can form manifolds of various topologies. Topological semimetallic states [9–15] in condensed-matter physics are excellent platforms for achieving emergent particles beyond the elementary particles in high-energy physics. Tens of thousands of topological semimetals [16,17] that host nontrivial emergent fermions, such as nodal point [18–25], nodal line [26–30], and nodal surface (NS) [31–35] fermions, have been proposed using the theory of symmetry indicators. Wu *et al.* [31] clarified the symmetry protection of NSs and summarized the classification of NSs in three-dimensional materials. However, the NSs of electrons may be influenced by the spin-orbit coupling (SOC). For example, the nonsymmorphic symmetry-dominated NSs in MSiS (M = Hf and Zr) [35] are reduced to nodal lines when SOC is considered. Moreover, although symmetry-dominated NSs can be found in some electronic systems, they are far from the Fermi level, hindering experimental detection.

In recent years, it has been discovered that in addition to low-energy electronic states, the phonons [36,37] in real materials also provide an excellent platform for obtaining emergent particles, including nodal line [38–40], nodal chain [41–43], nodal net [44], charge-four Weyl [45–47], double-Weyl [48–52], threefold degenerate nodal point [53], sixfold degenerate nodal point [54], one-NS, two-NS, and three-NS [55–58] phonons. As shown in Fig. 1(a), the one-NS phonons host one pair of NS states on the $k_i = \pm\pi$ ($i = x$, y, or z) planes. This year, Liu *et al.* [55] published a complete list of all the candidate SGs with one-NS phonons in 230 space groups (SGs). They stated that the SG with numbers 4, 11, 14, 17, 20, 26, 29, 31, 33, 36, 51–54, 63, and 64 are the hosts to achieve the one-NS phonons. Motivated by their work, we [57] extended the types of NS phonons from one- to three-NS phonons [see Fig. 1(c)]. The three-NS phonons [57] host three pairs of NS states on the $k_i = \pm\pi$ ($i = x$, y, and z) planes. We discovered that materials with SG Nos. 19, 61, 62, 92, 96, 198, 205, 212, and 213 have three-NS phonons. It should be noted that three-NS phonons can be viewed as an ideal platform for circumventing the no-go theorem and achieving single-Weyl point phonons [59]. Figure 1(b) shows two-NS phonons that

*These authors contributed equally to this work.
†ying_liu@hebut.edu.cn
‡xiaotianwang@swu.edu.cn

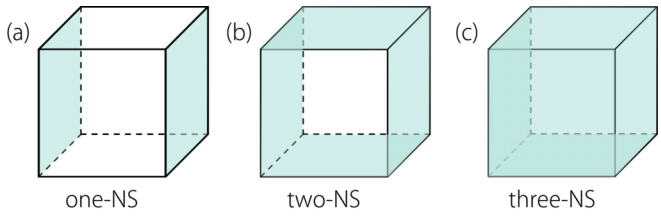

FIG. 1. (a)–(c) Schematics of one-NS, two-NS, and three-NS phonons, respectively. The NS states are highlighted by the green color.

host two pairs of NS states on two of three $k_i = \pm\pi$ ($i = x$, y, and z) planes. To this date, only a few realistic materials [58,60] with SG Nos. 137 and 136 have been proposed to have two-NS phonons. To provide comprehensive guidance for follow-up theoretical studies, we had to identify all possible two-NS phonons in 230 SGs. Moreover, the phonons follow the Bose-Einstein statistic without Fermi energy limitations, implying that two-NS phonons should be much more common in three-dimensional materials. Hence, we must propose as many material candidates with two-NS phonons as possible in order to assist follow-up experimental studies.

First, we present the symmetry condition for the occurrence of two-NS phonons in this paper. Second, we screen all 230 SGs for candidate groups that can host two-NS phonons. Third, we present a series of realistic materials with the candidate groups and with two-NS phonons. Finally, we examine the phonon dispersions of 10 037 materials listed in the phonon database at Kyoto University [61] and determine all the candidates with two-NS phonons. The authors hope that this comprehensive paper on two-NS phonons would guide future investigations in related fields.

II. SYMMETRY CONDITIONS FOR TWO-NS PHONONS

The NS is formed by band crossings that occur in two dimensions. It is worth noting that it is of double degeneracy. The category we examine here is a class-II NS [31] with a nonsymmorphic symmetry. This type of NS only occurs on the Brillouin zone (BZ) boundary plane, and it has linear dispersion along the direction normal to the surface. In this paper, we mainly focused on two-NS phonons with two pairs of NS states on two of three $k_i = \pm\pi$ ($i = x$, y, and z) planes. According to Wu *et al.* [31], such a surface is due to the combination of the twofold screw symmetry (S_{2i}) and time-reversal symmetry ($\mathcal{T}$). We considered a twofold screw rotation along the x direction, i.e., $S_{2x}: (x, y, z) \to (x + \frac{1}{2}, -y, -z)$, which is a nonsymmorphic symmetry with a half translation in the lattice constant along its rotation axis without losing generalization. Furthermore, S_{2x} inverses k_y and k_z only maintains k_x in the $\boldsymbol{k}$ space. One can conclude that in $S_{2x}^2 = T_{100} = e^{-ik_x}$, T_{100} is the translation along the x direction. Subsequently, we considered the $\mathcal{T}$ (note that for spinless systems, $\mathcal{T}^2 = 1$), which is an antiunitary operator that inverses the $\boldsymbol{k}$ momentum. The combination of S_{2x} and $\mathcal{T}$, i.e., $\mathcal{T}S_{2x}$, is also an antiunitary operator that only inverses k_x. On planes where $k_x = \pm\pi$, there is $(\mathcal{T}S_{2x})^2 = e^{-ik_x}|_{k_x=\pm\pi} = -1$, indicating a Kramer-like degeneracy on the $k_x = \pm\pi$ planes.

TABLE I. A complete list of candidates SGs with two-NS phonons in 230 SGs. The first and second columns present the SG numbers and symbols, the third column lists the NSs along the symmetry paths, and the fourth column presents the corresponding realistic materials. For SGs with Nos. 18 and 55–60, two pairs of NS states appear on the $k_x = \pm\pi$ and $k_y = \pm\pi$ planes. We only list two NSs (NS_{UXS} and NS_{TYS}) on the $k_x = \pi$ and $k_y = \pi$ planes in this table because the NSs on the $k_x = \pi$ and $k_y = \pi$ planes are equivalent to those on the $k_x = -\pi$ and $k_y = -\pi$ planes. For SGs with Nos. 90, 94, 113, 114, 127–130, and 135–138, two pairs of NS states appear on the $k_x = \pm\pi$ and $k_y = \pm\pi$ planes. Furthermore, we only display one NS (NS_{XRM}) at the $k_y = \pi$ because the NS on the $k_y = \pi$ plane is equivalent to those on the $k_x = \pm\pi$ and $k_y = -\pi$ planes.

Space numbers	SG symbols	Two-NSs	Realistic materials
18	$P2_12_12$	NS_{UXS} and NS_{TYS}	$ZnTeMo_6$
55	*Pbma*	NS_{UXS} and NS_{TYS}	Cs_2Te_2
56	*Pccn*	NS_{UXS} and NS_{TYS}	Sr_2SnO_4
57	*Pbcm*	NS_{UXS} and NS_{TYS}	CaAlPd
58	*Pnnm*	NS_{UXS} and NS_{TYS}	PtO_2
59	*Pmmn*	NS_{UXS} and NS_{TYS}	KLi_2As
60	*Pbcn*	NS_{UXS} and NS_{TYS}	CV_2
90	$P42_12$	NS_{XRM}	$BaVCu_4P_4O_{17}$
94	$P4_22_12$	NS_{XRM}	$Na_5Fe_3F_{14}$
113	$P\bar{4}2_1m$	NS_{XRM}	BaS_3
114	$P\bar{4}2_1c$	NS_{XRM}	Na_4SnS_4
127	$P4/mbm$	NS_{XRM}	ReO_3
128	$P4/mnc$	NS_{XRM}	$Sr_4Li_2Si_4N_8O$
129	$P4/nmm$	NS_{XRM}	$BaHfN_2$
130	$P4/ncc$	NS_{XRM}	Bi_2CuO_4
135	$P4_2/mbc$	NS_{XRM}	YB_2C
136	$P4_2/mnm$	NS_{XRM}	MgF_2
137	$P4_2/nmc$	NS_{XRM}	YB_4Rh_4
138	$P4_2/ncm$	NS_{XRM}	$LiClO_2$

For the two-NS phonons, the phonon bands along the symmetry paths of two of three pairs on $k_i = \pm\pi$ ($i = x, y, z$) planes are doubly degenerate. In this paper, we screened all 230 SGs for two-NSs phonons and concluded that the SG 18, 55–60, 90, 94, 113, 114, 127–130, and 135–138 candidates can host two-NSs phonons (see Table I). The presence of two twofold rotation symmetries, namely, S_{2x} and S_{2y} in the above-mentioned SGs will induce two pairs of NS states on the $k_x = \pm\pi$ and $k_y = \pm\pi$ planes [see Figs. 2(a) and 2(b)].

III. MATERIAL REALIZATIONS FOR TWO-NS PHONONS

To prove that two-NS phonons can exist in realistic materials with SG Nos. 18, 55–60, 90, 94, 113, 114, 127–130, and 135–138, we selected 19 material samples with the above-mentioned SG Nos., namely, $P2_12_12$-type $ZnTeMoO_6$ (with SG No. 18), *Pbma*-type Cs_2Te_2 (with SG No. 55), *Pccn*-type Sr_2SnO_4 (with SG No. 56), *Pbcm*-type CaAlPd (with SG No. 57), *Pnnm*-type PtO_2 (with SG No. 58), *Pmmn*-type KLi_2As (with SG No. 59), *Pbcn*-type CV_2 (with SG No. 60), $P42_12$-type $BaVCu_4P_4O_{17}$ (with SG No. 90), $P4_22_12$-type $Na_5Fe_3F_{14}$ (with SG No. 94), $P\bar{4}2_1m$-type BaS_3 (with SG No. 113), $P\bar{4}2_1c$-type Na_4SnS_4 (with SG No. 114), $P4/mbm$-type ReO_3 (with SG No. 127), $P4/mnc$-type $Sr_4Li_2Si_4N_8O$

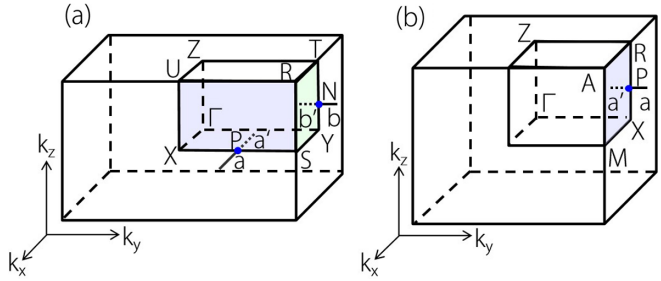

FIG. 2. Three-dimensional BZ and selected symmetry points, $U, X, S, R, Z, T, Y, \Gamma, a, P, a', b, N$, and b' for materials with SG Nos. 18 and 55–60. The purple and green colors indicate the two NS states (i.e., NS_{UXS} and NS_{TYS}) on the $k_x = \pi$ and $k_y = \pi$ planes, respectively; (b) three-dimensional BZ and selected symmetry points, $A, M, X, R, Z, \Gamma, a, P$, and a' for materials with SG Nos. 90, 94, 113, 114, 127–130, and 135–138. The purple color indicates the NS state (NS_{XRM}) on the $k_y = \pi$ plane.

(with SG No. 128), $P4/nmm$-type $BaHfN_2$ (with SG No. 129), $P4/ncc$-type Bi_2CuO_4 (with SG No. 130), $P4_2/mbc$-type YB_2C (with SG No. 135), $P4_2/mnm$-type MgF_2 (with SG No. 136), $P4_2/nmc$-type YB_4Rh_4 (with SG No. 137), and $P4_2/ncm$-type $LiClO_2$ (with SG No. 138), and individually described their two-NS phonons and preparation methods. The computational methods can be found in the Supplemental Material (SM) [62] (see, also, Refs. [63–67] therein).

The first example is $Pbma$-type Cs_2Te_2. Cs_2Te_2 has been obtained using several preparation methods. For example, it can be simply produced by reducing Cs_2Te_2O with hydrogen at 400 °C [68]. Figure 3(a) depicts the unit cell of Cs_2Te_2. The lattice constants and atomic positions of Cs_2Te_2 are totally relaxed based on first-principles calculations. The obtained lattice constants are $a = 5.104$, $b = 6.323$, and $c = 11.822$ Å, which agree well with the experimental data ($a = 4.960$, $b = 6.128$, and $c = 11.629$ Å). The Cs and Te atoms in Cs_2Te_2 occupy $4h$ and $4g$ Wyckoff positions, respectively. Based on the symmetry paths shown in Fig. 2(a), the phonon dispersion of Cs_2Te_2 along the Γ-X-S-Y-Γ-Z-U-X-S-R-T-Y-S paths is shown in Fig. 3(b). The phonon bands along the X-S-Y and U-X-S-R-T-Y-S paths are shown to be doubly degenerate. For clarity, we only focus on the two regions (along the U-X-S and T-Y-S paths) with purple and green boxes in the frequency range of 4.7–5.1 THz because the U-X-S and T-Y-S paths are located on the $k_x = \pi$ and $k_y = \pi$ planes, respectively. Figure 3(c) shows enlarged figures of the phonon bands in the purple and green boxes. Any point on the $k_x = \pi$ and $k_y = \pi$ planes is a twofold degenerate point with linear phonon band dispersions. As shown in Fig. 2(a), we chose two more points, P and N, on the X-S and T-Y paths, respectively, and built symmetry paths, a-P-a' and b-N-b', normal to the $k_x = \pi$ and $k_y = \pi$ planes, respectively. Figure 3(d) shows the phonon dispersions of Cs_2Te_2 along the a-P-a' and b-N-b' paths. The points at P and N are indeed twofold degenerate points with linear phonon band dispersion. The presence of NS states on the $k_x = \pi$ and $k_y = \pi$ planes can be deduced from Fig. 3(c). There are two additional NSs on the $k_x = -\pi$ and $k_y = -\pi$ planes because of the periodic property of the BZ.

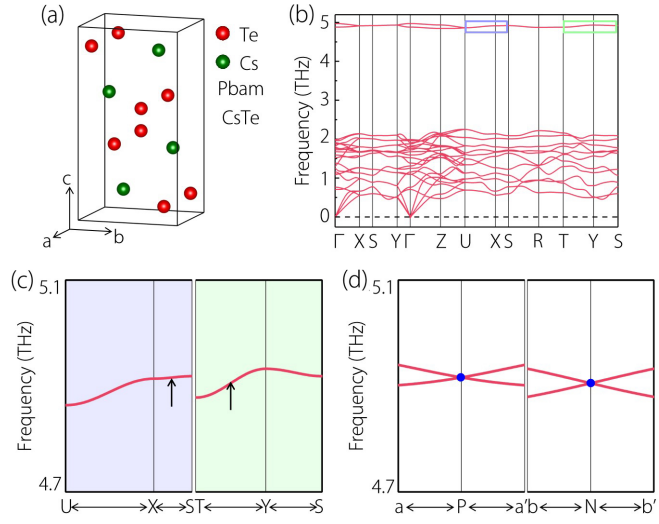

FIG. 3. Crystal structure of Cs_2Te_2, (b) calculated phonon dispersion of Cs_2Te_2 along the Γ-X-S-Y-Γ-Z-U-X-S-R-T-Y-S paths, (c) enlarged phonon dispersions along the U-X-S and T-Y-S paths, and (d) calculated phonon dispersions along the a-P-a' and b-N-b' paths.

The second example is the solid-state reaction-prepared polycrystalline $ZnTeMoO_6$ sample with a $P2_12_12$-type structure [69]. Zhu *et al.* [70] reported on its electrochemical performance in the energy storage field this year. Figure 4(a) depicts the unit cell of $ZnTeMoO_6$. Based on first-principles calculations, the lattice constants and atomic positions of $ZnTeMoO_6$ are totally relaxed. The Zn, Te, Mo, and O atoms in $ZnTeMoO_6$ occupy $2a$, $2b$, $2b$, and $4c$ Wyckoff positions, respectively. The third example is $Pccn$-type Sr_2SnO_4 (with SG No. 56), which can be prepared from $SrCO_3$ and SnO_2 in an alumina crucible [71]. Figure 4(b) depicts the unit cell of Sr_2SnO_4. The Sr and Se atoms occupy $8e$ and $4b$ Wyckoff positions, respectively, and the O atoms occupy the $8e$, $4c$, and $4d$ Wyckoff positions. The fourth example is $Pbcm$-type CaAlPd (with SG No. 57), which can be prepared by arc melting Ca, Al, and Pd elements [72]. Figure 4(c) depicts the unit cell of CaAlPd. The Ca, Al, and Pd atoms occupy the $4d$, $4d$, and $4c$ Wyckoff positions, respectively. The fifth example is $Pnnm$-type PtO_2, which can be obtained by heating any of the platinum starting materials at temperatures above 580 °C and high oxygen pressures [73]. Figure 4(d) depicts the unit cell of PtO_2. The Pt and O atoms occupy the $2b$ and $4g$ Wyckoff positions, respectively. The sixth example is $Pmmn$-type KLi_2As. KLi_2As [74] can be prepared either directly from its elements or by reacting the binary components, Li_3As and K_3As, under inert conditions. Figure 4(e) depicts the unit cell of KLi_2As. The K, Li, and As atoms occupy the $2a$, $4e$, and $2b$ Wyckoff positions, respectively. The seventh example is $Pbcn$-type CV_2 [75], which can be obtained by reacting a cold-pressed powder mixture of vanadium and graphite under protective gas (argon) at 1350 °C. Figure 4(f) depicts its unit cell. The V and C atoms occupy the $8d$ and $4c$ Wyckoff positions, respectively.

Figure 5 shows the phonon dispersions of the material samples (exhibited in Fig. 4) along the

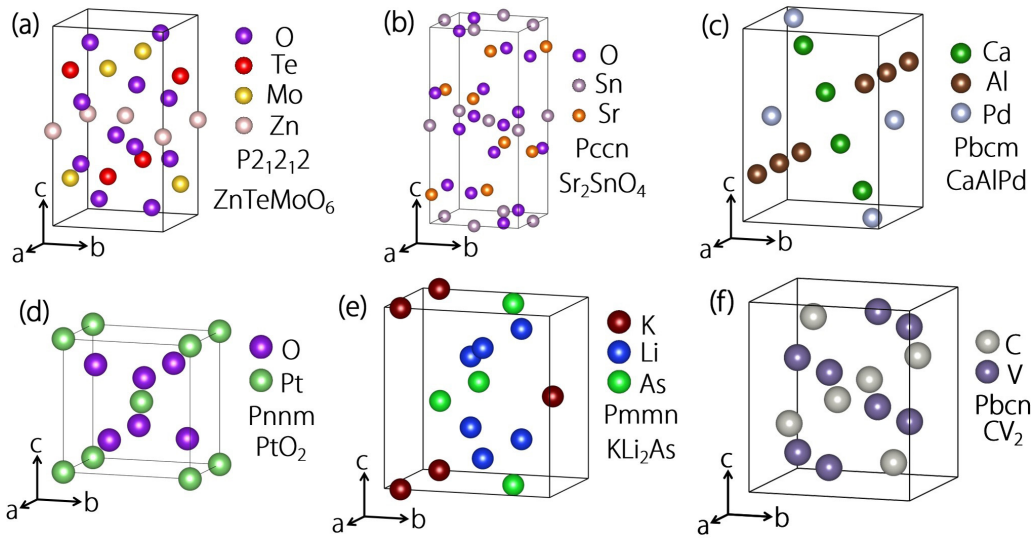

FIG. 4. (a)–(f) Crystal structures of $ZnTeMoO_6$, Sr_2SnO_4, CaAlPd, PtO_2, KLi_2As, and CV_2, respectively.

Γ-*X*-*S*-*Y*-Γ-*Z*-*U*-*X*-*S*-*R*-*T*-*Y*-*S* paths. Similar to the case of the Cs_2Te_2, the phonon bands along the *U*-*X*-*S* and *T*-*Y*-*S* paths are doubly degenerate, namely, these materials also have two-NS phonons on the $k_x = \pm\pi$ and $k_y = \pm\pi$ planes because they are protected by antiunitary symmetries $\mathcal{T}S_{2x}$ and $\mathcal{T}S_{2y}$.

As can be observed in the selected regions (the purple and green boxes) in Fig. 5, the NSs in Figs. 5(a), 5(d), and 5(e) are very clean, namely, no other topological signatures appeared around the frequencies of the boxes. Furthermore, the phonon bands that form the NSs are well separated from the phonon bands in other frequency regions.

As can be observed in Figs. 5(c) and 5(f), the twofold degenerate phonon bands (i.e., the NS states) along the *U*-*X*-*S* paths merged into a fourfold degenerate phonon band along the *S*-*R* path [see the black boxes in Figs. 5(c) and 5(f)]. Such a fourfold degenerate phonon band is indeed an open DNL along the *S*-*R* path for the CaAlPd and CV_2 materials [see the white lines in Figs. 6(a) and 6(b)]. The DNL is a one-dimensional fourfold degenerate band with a linear dispersion

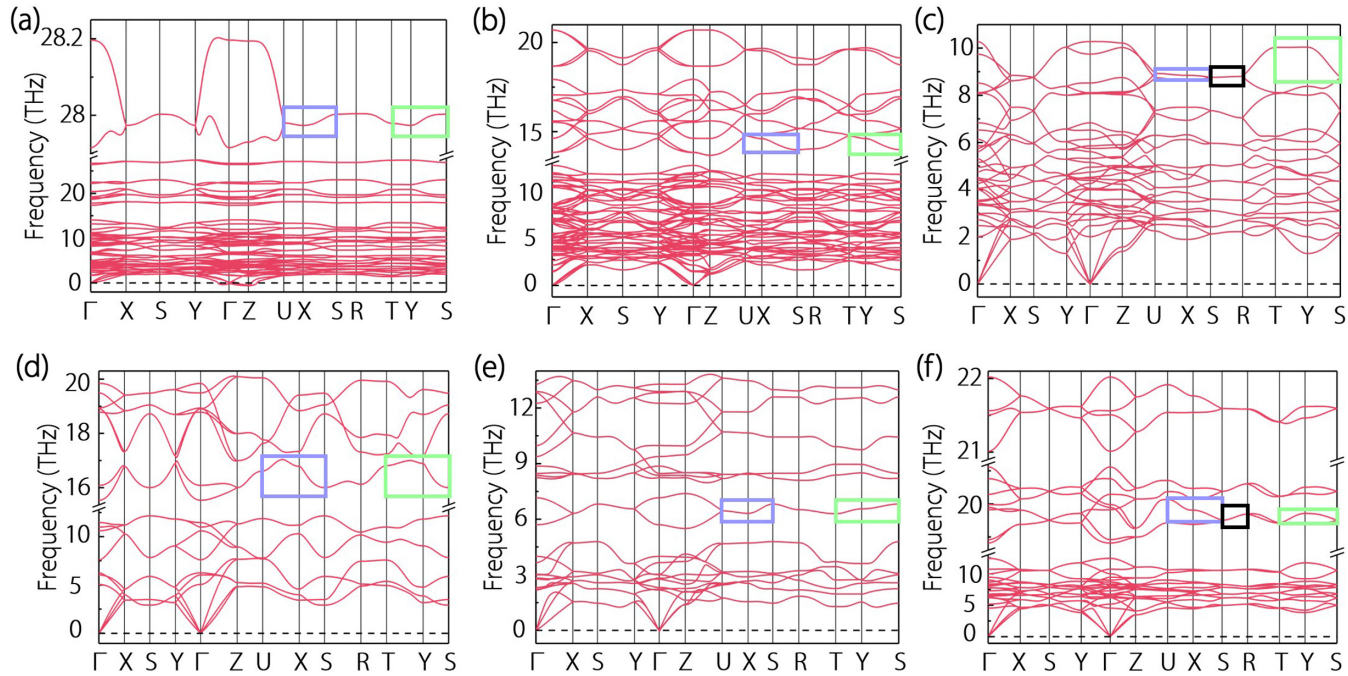

FIG. 5. (a)–(f) Calculated phonon dispersions for the $ZnTeMoO_6$, Sr_2SnO_4, CaAlPd, PtO_2, KLi_2As, and CV_2 materials along the Γ-*X*-*S*-*Y*-Γ-*Z*-*U*-*X*-*S*-*R*-*T*-*Y*-*S* paths. The purple and green boxes represent the NS states along the *U*-*X*-*S* and *T*-*Y*-*S* paths, respectively. The Dirac nodal line (DNL) phonons along the *S*-*R* path for the CaAlPd and CV_2 materials are marked with black boxes in (c) and (f), respectively.

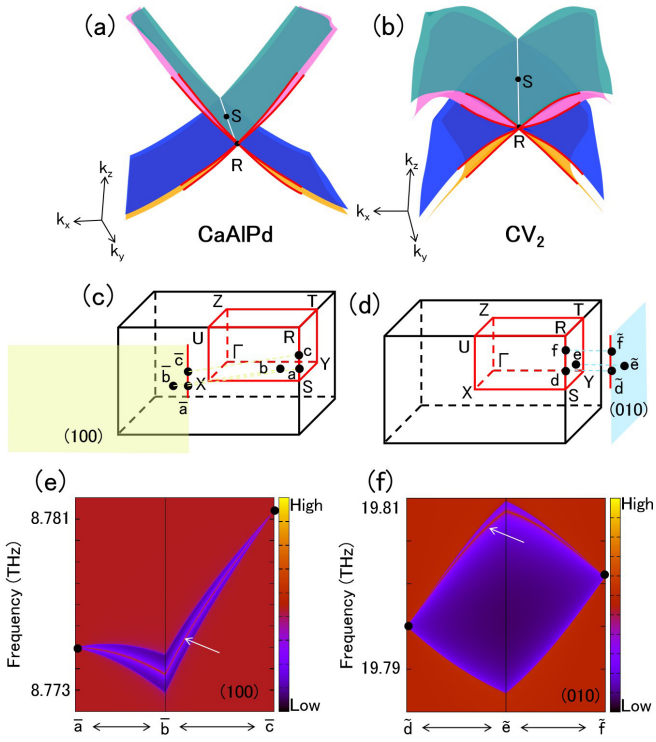

FIG. 6. Schematics of the DNLs for the (a) CaAlPd and (b) CV_2 materials. The DNLs are marked with white lines. (c) and (d) Three-dimensional BZs and the (100) and (010) surface BZs for the CaAlPd and CV_2 materials, respectively. The projections of the a, b, and c points are $\bar{a}$, $\bar{b}$, and $\bar{c}$ on the (100) surface, and the projections of the d, e, and f points are $\widetilde{d}$, $\widetilde{e}$, and $\widetilde{f}$ on the (010) surface. (e) and (f) The (100) and (010) phonon surface states for the CaAlPd and CV_2 materials, respectively. The phonon surface states are marked with white arrows, and the projections of the points are highlighted by black dots.

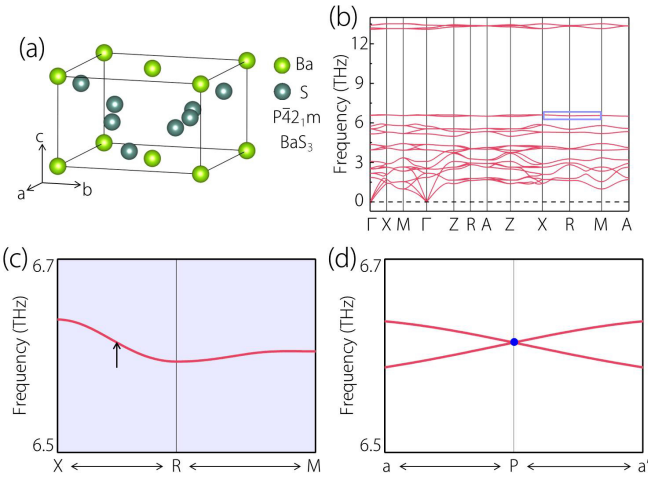

FIG. 7. Crystal structure of BaS_3, (b) calculated phonon dispersion of BaS_3 along the Γ-X-M-Γ-Z-R-A-Z-X-R-M-A paths, (c) enlarged phonon dispersion along the X-R-M paths, and (d) calculated phonon dispersions along the a-P-a' paths.

on the plane normal to the line [see the red lines in Figs. 6(a) and 6(b)]. For a better understanding of the DNL phonons along the S-R path, the following represents a brief symmetry analysis for the occurrence of DNL phonons in materials with SG. 57. Any state along this path can be chosen as the eigenstates of $M_y = \mathcal{P}S_{2y}$-$(x, y, z) \to (-x, y + \frac{1}{2}, -z + \frac{1}{2})$, which are denoted by their eigenvalues (g_y is denoted as $|g_y = \pm i\rangle$). Since the S-R path is invariant under $M_x = \mathcal{P}S_{2x}$, one may deduce that this path is also invariant under $\mathcal{T}M_z$ which is an antiunitary operator. Remarkably, $(\mathcal{T}M_z)^2 = e^{-ik_z} = -1$ along this path, suggesting that each band is, at least, doubly degenerate on this path. Furthermore, M_x anticommutes with M_y along this path, particularly $M_xM_y = e^{-ik_y}M_yM_x$ such that $\{M_x, M_y\} = 0$, doubling the degeneracy on this path. Consequently, this path is of fourfold degeneracy. The S-R path belonging to SG 60 can also be discussed in a similar manner.

The phononic surface states of the DNL along the S-R path in the CaAlPd and CV_2 materials were subsequently investigated. As shown in Figs. 6(c) and 6(d), we selected six points, i.e., a (0.5, 0.5, 0.2), b (0.5, 0.4, 0.2), c (0.5, 0.5, 0.25), d (0.5, 0.5, 0.24), e (0.4, 0.5, 0.25), and f (0.5, 0.5, 0.26) points, on the $k_y = \pi$ plane, plotted fa, b, and c to $\bar{a}$, $\bar{b}$, and $\bar{c}$ on the (100) surface, and plotted d, e, and f to $\widetilde{d}$, $\widetilde{e}$, and $\widetilde{f}$ in the (010) surface. The phononic surface spectra for both materials on the (100) and (010) surfaces were obtained by constructing the phonon tight-binding model. Figures 6(e) and 6(f) show the results. The positions of $\bar{a}$, $\bar{c}$, $\widetilde{d}$, and $\widetilde{f}$ are highlighted by black dots, and a and c (d and f) are the crossing points of the DNL along the S-R path for the CaAlPd and CV_2 materials, respectively. As shown in Figs. 6(e) and 6(d), the phononic surface states (marked with white arrows) connect the projections of the crossing points. We would like to point out that the DNL phonons and the (100) and (010) surface states for the CaAlPd and CV_2 materials are extremely clean, which aids experimental detections. The following techniques are recommended for detecting the clean phonon surface states of the CaAlPd and CV_2 materials: helium scattering, terahertz polarimetry, and high-resolution electron energy-loss spectroscopy.

Subsequently, we propose some realistic materials with two-NS phonons, and they have SG Nos. 90, 94, 113, 114, 127–130, and 135–138. Figure 2(b) depicts the three-dimensional BZ of these materials, which is different from that of materials with SG Nos. 18 and 55–60 [see Fig. 2(a)]. We selected the BaS_3 material as an example to determine its two-NS signature in phonons. Single crystals of BaS_3 [76] can be obtained by heating BaS with sulfur in quartz ampoules to 550 °C. Figure 7(a) shows the crystal structure of BaS_3. The Ba atoms occupy the $2a$ Wyckoff position, whereas the S atoms occupy the $2c$ and $4e$ Wyckoff positions. Figure 7(b) shows the phonon dispersion of BaS_3 based on the Γ-X-M-Γ-Z-R-A-Z-X-R-M-A symmetry paths. The theoretical lattice constants and the experimental lattice constants are in good agreement as listed in Table II (see Appendix A). The phonon bands along the X-R-M paths have a twofold degeneracy, as shown in Fig. 7(b). The X-R-M symmetry paths belong to the $k_y = \pi$ plane. For clarity, Fig. 7(c) shows the enlarged figure of the phonon bands with the purple box exhibited in Fig. 7(b). We selected the a-P-a' paths [see Fig. 2(b)], which are perpendicular to line R-X and normal to the $k_y = \pi$ plane, and calculated the phonon dispersion of BaS_3 along the a-P-a' paths. Figure 7(d) shows the results, which reveal that P is

TABLE II. The theoretical and experimental lattice constants for a series of selected realistic materials with two-NS phonons.

Materials	Theoretical lattice constants	Experimental lattice constants
$ZnTeMoO_6$	$a = 5.081,\ b = 5.339,\ c = 9.303$Å	$a = 5.025,\ b = 5.263,\ c = 8.911$ Å [69]
Cs_2Te_2	$a = 5.104,\ b = 6.323,\ c = 11.822$ Å	$a = 4.960,\ b = 6.128,\ c = 11.629$ Å [68]
Sr_2SnO_4	$a = 5.869,\ b = 5.885,\ c = 12.517$ Å	$a = 5.728,\ b = 5.735,\ c = 12.587$ Å [71]
CaAlPd	$a = 5.627, b = 5.764,\ c = 7.875$ Å	$a = 5.62,\ b = 5.75,\ c = 7.79$ Å [72]
PtO_2	$a = 3.192,\ b = 4.555,\ c = 4.611$ Å	$a = 3.138,\ b = 4.486,\ c = 4.537$ Å [73]
KLi_2As	$a = 4.472,\ b = 6.361,\ c = 6.702$ Å	$a = 4.458,\ b = 6.27,\ c = 6.715$ Å [74]
CV_2	$a = 4.555,\ b = 5.039,\ c = 5.735$ Å	$a = 4.577,\ b = 5.037,\ c = 5.742$ Å [75]
$BaVCu_4P_4O_{17}$	$a = b = 9.773,\ c = 7.358$ Å	$a = b = 9.559,\ c = 7.16$ Å [77]
$Na_5Fe_3F_{14}$	$a = b = 7.667,\ c = 10.269$ Å	$a = b = 7.345,\ c = 10.490$ Å [78]
BaS_3	$a = b = 6.982,\ c = 4.237$ Å	$a = b = 6.881,\ c = 4.177$ Å [76]
Na_4SnS_4	$a = b = 7.938,\ c = 7.007$ Å	$a = b = 7.837,\ c = 6.95$ Å [79]
ReO_3	$a = b = 5.368,\ c = 3.790$ Å	$a = b = 5.297,\ c = 3.742$ Å [80]
$Sr_4Li_2Si_4N_8O$	$a = b = 9.382,\ c = 5.612$ Å	$a = b = 9.296,\ c = 5.553$ Å [81]
$BaHfN_2$	$a = b = 9.296,\ c = 5.553$ Å	$a = b = 4.127,\ c = 8.381$ Å [82]
Bi_2CuO_4	$a = b = 8.518,\ c = 6.038$ Å	$a = b = 8.506,\ c = 5.822$ Å [83]
YB_2C	$a = b = 6.802,\ c = 7.497$ Å	$a = b = 6.793,\ c = 7.438$ Å [84]
MgF_2	$a = b = 4.670,\ c = 3.077$ Å	$a = b = 4.621,\ c = 3.051$ Å [85]
YB_4Rh_4	$a = b = 5.347,\ c = 7.474$ Å	$a = b = 5.308,\ c = 7.403$ Å [86]
$LiClO_2$	$a = b = 4.831,\ c = 10.688$ Å	$a = b = 4.722,\ c = 10.298$ Å [87]

a twofold degenerate crossing point with linear dispersion because of the Kramers degeneracy. Actually, the twofold Kramers degeneracy arises at every point on the $k_y = \pi$ plane, resulting in a symmetry-dominated NS on the $k_y = \pi$ plane. As shown in Fig. 7(c), the NS is very flat with frequency variations of less than 0.1 THz (approximately 0.4 meV). It is worth noting that equivalent NS states can also be found on the $k_x = \pm\pi$ and $k_y = -\pi$ planes because of the S_{4z} symmetry.

In addition to BaS_3, eleven other materials with the same three-dimensional BZ are proposed in this paper as materials with two-NS phonons. Figures S1(a)–S11(a) (in the Supplemental Material [62]) show the crystal structures of the 11 materials. Single crystals of $P42_12$-type $BaVCu_4P_4O_{17}$ [77] can be produced via solid-state reactions just below the melting points of the reaction mixtures of BaP_2O_6, $C_3(PO_4)_2$, CuO, V_2O_5, and V_2O_3 in closed evacuated quartz glass tubes. Powdered $P4_22_12$-type $Na_5Fe_3F_{14}$ [78] can be obtained from a stoichiometric mixture of 5NaF + 3FeF, which is heated to 650 °C in a sealed gold tube under argon atmosphere. $P\bar{4}2_1c$-type Na_4SnS_4 microcrystals [79] can be synthesized in vacuum-sealed silica tubes. ReO_3 [80] can be obtained via an iodine chemical transport reaction. At ambient pressure, the cubic $Pm3m$ phase is the ground state, but at 5.2 kbars, $P4/mbm$-type ReO_3 appears. $P4/mnc$-type $Sr_4Li_2Si_4N_8O$ [81] can be obtained from Li_2O, Sr, $Si(NH)_2$, and LiN_3 in liquid lithium. $P4/nmm$-type $BaHfN_2$ [82] can be produced via the high-temperature solid-state reaction of Ba_3N_2 and HfN powders. $P4/ncc$-type Bi_2CuO_4 [83] can be synthesized by directly reacting CuO with Bi_2O_3 in alumina crucibles. $P4_2/mbc$-type YB_2C [84] can be obtained by reacting stoichiometric mixtures of the Y, B, and C elements. $P4_2/mnm$-type MgF_2 [85] occurs in nature. $P4_2/nmc$-type YB_4Rh_4 [86] can be obtained by arc melting. $LiClO_2$ [87] can be synthesized by mixing aqueous solutions of barium chloride and Li sulfates in equimolar ratios.

Figures S1–S11 (in the Supplemental Material [62]) illustrate the phonon dispersions of these materials along the Γ-X-M-Γ-Z-R-A-Z-X-R-M-A paths. As shown in the figures, the phonon bands along the X-R-M paths are doubly degenerated (see the purple boxes) for all the materials. Hence, similar to BaS_3, all these materials have two-NS phonons on the $k_x = \pm\pi$ and $k_y = \pm\pi$ planes.

IV. MATERIAL CANDIDATES WITH TWO-NS PHONONS

The NS states in electronic systems are normally located around the Fermi level and are formed by the crossing of conduction and valence bands. This condition imposes constraints regarding the electron filling of the bands. Since the phonons follow the Bose-Einstein statistic without the limitation of Fermi energy. That is, in principle, the NS states can be detected in the whole frequencies of the phonon dispersion. Hence, phonons with NS states may exist much more universally in many materials than electrons with NS states.

To support the inspirational findings of two-NS phonons, we screened all 10 037 materials listed in the phonon database at Kyoto University [61] and discovered that 622 of them have two-NS phonons. Table III in Appendix B lists the selected 622 material candidates. Unfortunately, material candidates with SG Nos. 90 and 94 are missing (see Table III in Appendix B) in the phonon database at Kyoto University.

V. CONCLUSIONS

Based on the symmetry conditions, we obtained all the possible candidate SGs with two-NS phonons in the BZ of all 230 SGs. We discovered 19 candidate SGs (with Nos. 18, 55, 56, 57, 58, 59, 60, 90, 94, 113, 114, 127, 128, 129, 130, 135, 136, 137, and 138) that have two-NS phonons. By screening all 10 037 materials listed in the phonon database at Kyoto University [61], we discovered

TABLE III. The 622 out of 10 037 materials in the phonon database at Kyoto University [61] that were selected as materials with two-NS phonons. The materials' ids are shown in this table. The symbol (*) shows the materials are with imaginary frequencies in their phonon spectra.

SG numbers	Materials
18	$Nb_2Te_3O_{11}$(id: 27322*), $Sr_5Zr_3F_{22}$(id: 29085*), $Re_3Te_8Cl_3$(id: 29499*), La_3InS_6(id: 540877), $K_9Bi(PS_4)_4$ (id: 554554*), $Na_3BeAl(SiO_4)_2$(id: 556258), BaS_3(id: 556296), $KLaSi(CN_2)_4$(id: 567129), Sr_2SnSe_5(id: 568525), $Sb_6Pb_6S_{17}$(id: 630376*), Nb_2PS_{10}(id: 648932), $LiTi_2(PO_4)_3$(id: 773843*)
55	$Ta_2Pt_3Se_8$(id: 4425), $Ta_2Pd_3Se_8$(id: 18010), $Nb_2Pd_3Se_8$(id: 504898), $Ta_2Pt_3S_8$(id: 560046), Ca_2SnO_4(id: 4747), Sr_2PbO_4(id: 20944), Ca_2PbO_4(id: 21137), Na_2MgCl_4(id: 28657), Na_2CdCl_4(id: 28658), Na_2UO_4(id: 554191), Ca_2HfO_4(id: 752413), Sr_2HfO_4(id: 752537), Ba_4P_3(id: 28823), $CaGe_2O_5$(id: 4279), $K_3Sb_5O_{14}$(id: 12156*), $Rb_3Sb_5O_{14}$(id: 556234*), $Mg_{14}Ge_5O_{24}$(id: 27295), $Mg_{14}Si_5O_{24}$(id: 28663), $RbCO_2$(id: 556872),KCO_2(id: 560616), $K_3Nd(Si_2O_5)_3$(id: 6453*), RbTe(id: 8360), $HfPbO_3$(id: 22734*), $Al_4Bi_2O_9$(id: 23426), $K_2HgH_2Cl_4O$(id: 23926), $Zn_3(AsO_3)_2$(id: 27580*), $Tl_3Cd_2I_7$(id: 28432*), Ca_2CeO_4(id: 755597), Tl_4PbI_6(id: 29212), Sr_4As_3(Id: 29424), $Rb_5Au_3O_2$(id: 29920), $K_2U_7O_{22}$(id: 540610*), $SrGaBO_4$(id: 554053*), $NaTi_2Ga_5O_{12}$(id: 554441*), $Er_2B_2Cl_2O_5$ (id: 556986), $AgHg_2AsO_4$(id: 558188), $K_5Au(IO)_2$(id: 558332), $NaTi_2Al_5O_{12}$(id: 560591), $SiAs_2$(id: 978553), $Sr_4Sn_2Se_9$(id: 570983), $In_2Bi_4Pb_4S_{13}$(id: 650840), $Ba_2Sc_2O_5$(id: 755950), CuHgSeCl(id: 569687*)
56	Sb_2O_3(id: 2136), Bi_2O_3(id: 556549), SiO_2(id: 557465), $Ca(BO_2)_2$(id: 8056), $Rb_5H_5(OF_3)_2$(id: 555178), $Zn_2TeCl_2O_3$ (id: 557130*), $Zn_2TeBr_2O_3$(id: 558350), H_5CNO_3(id: 560121*), $KZn_4(PO_4)_3$(id: 560419*), $Zn_2B_2PbO_6$(id: 560471*), Na_2UO_4(id: 669528)
57	Sm_2SiTeO_4(id: 6055), Er_2SiSeO_4(id: 17633), Pr_2SiTeO_4(id: 17750), La_2SiSeO_4(id: 17834), Tb_2SiSeO_4(id: 17913), Dy_2SiSeO_4(id: 18219), Nd_2SiSeO_4(id: 18466), Nd_2SiTeO_4(id: 18542), Ho_2SiSeO_4(id: 18584), Sm_2SiSeO_4(id: 18610), $SrUO_4$(id: 3311), $BaUO_4$(id: 5611), $BaTiOF_4$(id: 16915), $HgHClO_4$(id: 24294), $RbTlF_4$(id: 27210*), $CaNb_2O_4$ (id: 29792), $UPbO_4$(id: 504922*), Ca_2AsClO_4(id: 560595), $SrNb_2O_4$(id: 768342), $UTeO_5$(id: 3516*), Sr_5NbN_5 (id: 10577), $SrSbF_5$(id: 16903*), TlF(id: 720), $BaSbF_5$(id: 18099), PBr_5(id: 22874*), $NaUBO_5$(id: 557744*), $NaNbO_3$(id: 3671*), $NbAgO_3$(id: 5537*), $LaAuO_3$(id: 28853), K_2HgS_2(id: 28859*), $La_5B_4N_9$(id: 29594), $KAsO_2$ (id: 30298*), $RbAsO_2$(id: 30299*), $Zr(TeCl)_6$(id: 31304), $Hf(TeCl)_6$(id: 31305), Cs_2Te_{13}(id: 505464), $Hg_7Cl_2O_3$ (id: 541193*), $Cu_2P_8Se_3I_2$(id: 570817), $Li_2Si_3O_7$(id: 555899*), $BaCu_6(GeS_4)_2$(id: 556714), $MgUB_2O_7$(id: 557384), PbO(id: 20878*), $SrLi_4Ca(SiO_4)_2$(id: 555089), $TlHg_3Sb_2Br_3$(id: 571582*), $TlHg_3As_2Cl_3$(id: 628647), $NaHCN_2$ (id: 634434), $Na_4AlP_2HO_9$(id: 741045), $Zn_2Hg_2H_2Se_2O_{11}$(id: 759925*), $LiNbO_3$(id: 776108*)
58	P_2Ru(id: 1413), FeS_2(id: 1522), P_2Os(id: 2319), As_2Os(id: 2455), FeP_2(id: 20027), $YbBr_2$(id: 22882), $CaBr_2$ (id: 22888), $CaCl_2$(id: 23214), SnO_2(id: 550172), Na_2O(id: 755072), $K_2Na_3TlO_4$(id: 17375*), SiO_2(id: 558025*), Al_2SiO_5(id: 4753), Sm_3InS_6(id: 21604), Sm_3InSe_6(id: 21562), Pr_3InSe_6(id: 21575), $Ba_3Al_2F_{12}$(id: 3361), $Mg_3(BO_3)_2$ (id: 5005), $Cd_3(BO_3)_2$(id: 5560), $Sr_2Li_3NbN_4$(id: 541568), $Rb_2Na_3InO_4$(id: 504851), $Pr_2Ta_3(SeO_4)_2$(id: 6105), GaTeCl(id: 27449), InS(id: 19795), $Ba_4Sb_4Se_{11}$(id: 28238*), $Sr_3(InP_2)_2$(id: 28324), Tl_2CuI_3(id: 28584), $NaSn_2Cl_5$ (id: 28947*), P_4N_6O(id: 28950*), $Nb_3Cl_5O_2$(id: 29924), $Be_2Te_7Cl_6$(id: 30096*), $Ca_3(BN_2)_2$(id: 531265), $Na_2Li_3GaO_4$ (id: 540945), $RbNa_2AuO_2$(id: 555018), $Rb_3Cu_2(BiS_2)_5$(id: 555113*), $K_3Y(BO_3)_2$(id: 555495), $K_3Cu_2(BiS_2)_5$ (id: 556522*), $Li_4Ca(BO_3)_2$(id: 557467), $KMg_4(PO_4)_3$(id: 557844), KNa_2AuO_2(id: 559067), $Li_5SbS_3I_2$(id: 559814), $Mg_{10}Ge_3(H_2O_9)_2$(id: 560872), Bi_6Cl_7(id: 582968*), $InHO_2$(id: 632711*), $Cs_3Cu_2(BiS_2)_5$(id: 669419*), $Mg_{10}Si_3(H_2O_9)_2$(id: 695890), Zn_2AsHO_5(id: 721702*), Tb_2SeO_2(id: 754218*), $Ba_2Ga_6O_{11}$(id: 778485*), AlH_3 (id: 570130*), $Ba_3(BO_3)_2$(id: 779608*)
59	ZrIN(id: 23052*), InClO(id: 27702), InBrO(id: 27703), TiBrN(id: 27849*), TiNCl(id: 27850*), AlClO(id: 27863), ErSeI(id: 28458), ScBrO(id: 546279*), HfBrN(id: 568346*), ZrBrN(id: 570157*), HoBrO(id: 752637*), TmClO (id: 754113), ErClO(id: 755689), K_3Ge_4Au(id: 17112), Na_5InO_4(id: 8840), Rb_3Ge_4Au(id: 17830), K_3Sn_4Au (id: 18500), Cs_3Ge_4Au(id: 510341), $BaTi_4O_9$(id: 3175), Li_5ReN_4(id: 3838), $KSbF_4$(id: 5079*), Li_5AlO_4(id: 7535), KNa_2BO_3(id: 8263), KLi_2As(id: 28994), $RbNO_3$(id: 13658*), $K_6Sn_3As_5$(id: 28728), $RbNa_2BO_3$(id: 8872), $Tl_2Au_4S_3$ (id: 29898), $K_2UAs_2O_9$(id: 558707*), $La_2TaCl_3O_4$(id: 559822*), $LiTa_3O_8$(id: 559908*), $CsMgH_3$(id: 571020), Cs_5YO_4(id: 769228*), $NaNb_3O_8$(id: 623854*), Li_5InO_4(id: 753783*), $Sr_3U_{11}O_{36}$(id: 667349*), $Sr(RhO_2)_2$ (id: 766173), $Cs_2UP_2O_9$(id: 561356*), Rb_3Sn_4Au(id: 17401*)
60	TiO_2(id: 1439), ZnF_2(id: 7709), MgH_2(id: 23711), SnO_2(id: 555487), MgH_2(id: 569051), $YbBr_2$(id: 571232), $CaCl_2$ (id: 571642),TiO_2(id: 775938*), HfO_2(id: 776097), Na_3P_{11}(id: 473), $SrTeO_4$(id: 4274), Th_2S_5(id: 1666), Rh_2O_3 (id: 1716), PPdSe(id: 3123), K_3P_{11}(id: 1568), $Ca(BO_2)_2$(id: 3417), $Li_2Si_2O_5$(id: 3552), $TlAg_3S_2$(id: 4762*), $MgSiO_3$(id: 5026), $MgTe_2O_5$(id: 5746), $Li_2Ge_7O_{15}$(id: 5832*), $Na_2Ti_2Si_2O_9$(id: 5996), $Nd_4Au_2O_9$(id: 3374), $Ca_2CO_3F_2$(id: 6246*), PPdS(id: 7280), $BaSi_2(NO)_2$(id: 6764*), $RbNaSnF_6$(id: 8333*), $LiInF_4$(id: 8892), $TaAlO_4$ (id: 8898), $Ba_2YC_2(O_2F)_3$(id: 8985), $La_4Au_2O_9$(id: 9160), $Sr(BO_2)_2$(id: 9749), $MgSe_2O_5$(id: 16771), Ge_3Os_2 (id: 16610), Si_3Os_2(id: 16608), $CsNaSnF_6$(id: 14380*), $Sm_4Au_2O_9$(id: 16160), Na_2MgPO_4F(id: 11165), $CaTeO_4$ (id: 12221), $Na_2Si_2O_5$(id: 16970), $CaNb_2O_6$(id: 17101*), Nb_2ZnO_6(id: 17177*), Ta_2ZnO_6(id: 17765*), $MgNb_2O_6$ (id: 17953*), NaTe(id: 28353), $Li_2Mg_2(SO_4)_3$(id: 14646), Si_3Ru_2(id: 22192), $BaZnCl_4$(id: 23522), Na_2TeO_4(id: 27537), Na_2PbO_2(id: 27622*), K_2CdO_2(id: 27742), Rb_2CdO_2(id: 28364), $ZnSe_2O_5$(id: 18373), Na_5InTe_4(id: 28597), $Na_7Au_5S_6$(id: 28856), Hg_2P_3Br(id: 28874), Nd_2NCl_3(id: 28970), $NaLuCl_4$(id: 29001), $Rb_2Hg_3Te_4$(id: 29107), $BaPdCl_4$(id: 30102), $Tb_2Ba_3(PS_4)_4$(id: 554264), $CdGe(BiO_3)_2$(id: 555027*), $Pb_2CO_3F_2$(id: 555946*), $LiNdGeO_4$ (id: 556814), $K_3Na_3(NO_4)_2$(id: 557181), $AlBPbO_4$(id: 558137*), $Ba_3Ho_2(PS_4)_4$(id: 559171), $Tb(BO_2)_3$(id: 559434),

TABLE III. (*Continued*.)

SG numbers	Materials
	$NaScCl_4$(id: 29432), $Nd_2Ti_3(ClO_4)_2$(id: 559560*), $LiAl(PO_3)_4$(id: 559987*), $Ba_3Er_2(PS_4)_4$(id: 560534), $Ba_3Dy_2(PS_4)_4$ (id: 560798), $Na_2Zn_5(PO_4)_4$(id: 560934*), $Al_2Si_2Pb_2O_9$(id: 561246*), $NbBi_4BrO_8$(id: 561382*), $CaAsH_3O_5$ (id: 721328*), Ca_3N_2(id: 568293), Ca_7GeN_6(id: 570555), $Na_2ZnGe_2(HO_2)_4$(id: 699457), $LiAgF_4$(id: 752460*), Li_3CuS_2(id: 753737), $SrCaI_4$(id: 754885), $BaTeO_4$(id: 754967), K_2MgO_2(id: 755802), Rb_2MgO_2(id: 756372), Ba_2SrI_6(id: 756624), Ba_2CaI_6(id: 766340*), LiCuS(id: 766467), $Ho_2(SO_4)_3$(id: 768800*), $Ca_4Ta_2O_9$(id: 769301), Sr_2CaI_6(id: 756798), Ta_2PbO_6(id: 771771*), $Li_2Ti_2O_5$(id: 772049), Sr_7GeN_6(id: 568436), $Na_2Ge_2O_5$(id: 772863*), $BaSr_2I_6$(id: 772876*), $Na_4P_3H_3O_{11}$(id: 774455*), $Na_2Ti_2O_5$(id: 781948), Na_2SnO_2(id: 778057*), $SrCa_2I_6$(id: 780396), Nb_2CdO_6(id: 781861*), $Ca_5Al_2(SiN_4)_2$£¨id: 866314), $Na_3Zn_4P_4H_4NO_{16}$(id: 772852*), $CdSiO_3$(id: 776023*)
90	None
94	None
113	$Ca_2MgSi_2O_7$(id: 6094*), $Ca_2BeSi_2O_7$(id: 6208), $Ca_2ZnSi_2O_7$(id: 6227*), $Sr_2MgSi_2O_7$(id: 6564), $Y_2Be_2SiO_7$(id: 6655) $Ho_2Be_2SiO_7$(id: 7013), $Nd_2Be_2SiO_7$(id: 9077), $Ba_2MgSi_2O_7$(id: 9338), $Pr_2Be_2GeO_7$(id: 14415), $Sm_2Be_2GeO_7$ (id: 14416), $Sr_2ZnGe_2O_7$(id: 17392), $La_2Be_2GeO_7$(id: 19926), $Dy_2Be_2GeO_7$(id: 20778), $Y_2Be_2GeO_7$(id: 541040), $Ca_2Al_2SiO_7$(id: 559691), Rb_3Ge_4Au(id: 17830), $Ca_2SiB_2O_7$(id: 752851), $TbAgTe_2$(id: 3551), $DyAgTe_2$(id: 4024), $ErAgTe_2$(id: 12902), $YAgTe_2$(id: 12903), $HoAgTe_2$(id: 12904), BNF_8(id: 4674), $Y_2Si_3N_4O_3$(id: 6941), $BaSe_3$(id: 7548), $BaTe_3$(id: 8234*), H_4CN_2O(id: 23778), $Ba_2ZnGe_2S_6O$(id: 17244), $La_2ZnGa_2S_6O$(id: 18129), $Sr_2MgGe_2O_7$(id: 972387), $Li_6Si_2O_7$(id: 27767), $PICl_6$(id: 27824*), $NbCl_3O$(id: 556422*), $NbBr_3O$(id: 606393*), $SbOF_3$(id: 758096*), $Na_4Al_4H_{10}O_{13}$(id: 758693*)
114	Na_3PO_4(id: 4223), Bi_2O_3(id: 23195*), $TlPO_3$(id: 27144*), $Si_2H_2S_3$(id: 28090), $H_2Pb_3O_4$(id: 28475), $S_2O_5F_2$ (id: 28676*), Na_4SnSe_4(id: 28768), Na_3PS_4(id: 28782), Na_3VS_4(id: 29143), Na_4SnS_4(id: 29628), $Sn_3(HO_2)_2$ (id: 625541), $Ag_2H_{12}S(NO)_4$(id: 723002), $Na_5ScH_4(C_2O_7)_2$(id: 24144*)
127	$CsRb_2PdF_5$(id: 8202*), $BaNd_2PdO_5$(id: 8514), $BaSm_2PdO_5$(id: 8515), $BaLa_2PtO_5$(id: 8809), CsK_2PdF_5(id: 8959), BaY_2PdO_5(id: 9656), $BaSm_2PtO_5$(id: 9757), $BaPr_2PdO_5$(id: 9759), Tb_2BaPdO_5(id: 9760), Rb_3PdF_5(id: 8201*), $BaNd_2PtO_5$(id: 556525), $NaBi_2AuO_5$(id: 557498*), K_3H_5Pd(id: 642736), K_3H_5Pt(id: 642821), Rb_3H_5Pt(id: 642845), Cs_3H_5Pt(id: 643005), $KAlF_4$(id: 2910*), Rb_3H_5Pd(id: 643022), Cs_3H_5Pd(id: 643006), $NaNbO_3$(id: 4419*), $NaTaO_3$ (id: 4675*), $RbAlF_4$(id: 5259*), $BaHo_2PdO_5$(id: 9785), $CsRb_2SiF_7$(id: 7380), $Ba_3In_2F_{12}$(id: 28274), $KAuSe_2$(id: 29138), Rb_2IN_3(id: 29456), $SrHfO_3$(id: 550908*), $CsSnI_3$(id: 616378*), $BaHg_2(ClO)_2$(id: 555736), $K_2LaNb_5O_{15}$(id: 559549*), $Ba_3Y_2F_{12}$(id: 752420*), $Ba_3La_2Cl_{12}$(id: 771914*), $Ba_3La_2Br_{12}$(id: 771951*), $Mg_2AlB_2Ir_5$(id: 865047*), Cs_3SiF_7(id: 13748*)
128	$Na_5Al_3F_{14}$(id: 4752*), K_2HfF_6(id: 8590*), K_2TeBr_6(id: 23411*), $Na_5Al_3H_{14}$(id: 24822), Tl_4HgI_6(id: 27375), Rb_2TeI_6 (id: 28070*), K_2PtI_6(id: 28247*), Tl_6SeI_4(id: 28517), Tl_2TeBr_6(id: 31076*), Tl_4CdI_6(id: 570339), $Zr(InBr_3)_2$ (id: 610738*), $Cd(In_2I_3)_2$(id: 616218)
129	KLiTe(id: 4495), NaZnP(id: 4824), CsNaTe(id: 5339), NaMgAs(id: 5962), KNaO(id: 6948*), KMgSb(id: 7089), NaMgSb(id: 7090), LaOF(id: 7100), NaCuTe(id: 7434*), ThSeO(id: 7950), NaLiS(id: 8452), RbNaO(id: 8453), CsNaSe(id: 8658), RbLiS(id: 8751), KLiSe(id: 8756), RbNaS(id: 8799), RbLiSe(id: 9250), RbCaAs(id: 9845), LiBeP(id: 9915), YOF(id: 10219), ErSF(id: 10932), NdSeF(id: 12620), NdTeF(id: 12621), KAgSe(id: 16236), BiClO(id: 22939), BaIF(id: 22951), SrClF(id: 22957), PbClF(id: 22964), PbIF(id: 22969), BiIO(id: 22987), PbBrF(id: 23008), LaBrO(id: 23023), SrBrF(id: 23024), LaClO(id: 23025), SrIF(id: 23046), NdClO(id: 23058), NdBrO(id: 23068), BaBrF(id: 23070), BiBrO(id: 23072), BaClF(id: 23432), LiHO(id: 23856*), CaHCl(id: 23859), SrHCl(id: 23860), BaHCl(id: 23861), BaHI(id: 23862), CaHI(id: 24204), SrHI(id: 24205), CaHBr(id: 24422), SrHBr(id: 24423), BaHBr(id: 24424), TmIO(id: 27439), CaClF(id: 27546), SmClO(id: 27823), PrClO(id: 27984), YClO(id: 27985), ThNCl(id: 28065), ThBrN(id: 28066), ThIN(id: 28067), LaHO(id: 28255), PrIO(id: 29254), SmBrO(id: 29327), HoClO(Id: 29731), LaIO(id: 30993), YbClF(id: 557483), HoIO(id: 753173), BiOF(id: 23074*), YIO(id: 753712), SmIO(id: 754217), TmBrO(id: 754969), DyClO(id: 755323), NdIO(id: 755336), YBrO(id: 768906), KCaBi(id: 773137), LuIO(id: 973585), LuBrO(id: 973981), PrBrO(id: 975666), SbBrO(id: 989189), SnClF(id: 989192*), SnBrF(id: 989193*), SbClO(id: 989196), SnO(id: 2097*), $BaZrN_2$(id: 3104), $NbPO_5$(id: 4888), Na_2TiSiO_5(id: 6138), Na_2TiGeO_5(id: 6228), Li_2TiSiO_5(id: 6332*), $NaLaTiO_4$(id: 6514), $LiLaTiO_4$(id: 6521), LaZnPO(id: 7060), $SrTiN_2$ (id: 9517), SnSe(id: 8936), SmCuSeO(id: 9194), DyCuSeO(id: 9304), NdZnAsO(id: 7061), $LiNdTiO_4$(id: 10520), $KNaLaNbO_5$(id: 10942), Cd_3SiO_5(id: 13820), $TaPO_5$(id: 15844), BaAgTeF(id: 167420, PbO£¨id: 19921), YZnAsO (id: 546011), SrCuSeF(id: 21228), PH_4I(id: 24409), PH_4Br(id: 27689), Ba_2InO_3F(id: 19956), LaCuTeO(id: 546790*), LaZnAsO(id: 549589), LaCuSeO(id: 552488), $BaPb_2BrF_5$(id: 554116), $BaPb_2IF_5$(id: 554245), Ba_2InBrO_3(id: 555212), CuBr(id: 22917), KNaSmNbO$_5$(id: 556438), RbNbAsClO$_5$(id: 556645)
130	Tl_4SnS_3(id: 9622*), Cs_3MgH_5(id: 23947), Rb_3MgH_5(id: 23948), $Sr(H_9O_5)_2$(id: 24312*), Tl_5Se_2Cl(id: 28920), Na_2PdCl_4 (id: 29359), K_3IO_5(id: 540618*), $La_5Sb_4(O_4F)_3$(id: 559298*), $K_5H(CN_2)_2$(id: 777297), Ba_3GeO_5(id: 778602)
135	SeO_2(id: 726), $Zn(SbO_2)_2$(id: 5388*), $Ti(SnO_2)_2$(id: 18288*), $Sn(PbO_2)_2$(id: 22467*), Pb_3O_4(id: 22633*), LiHS (id: 30959*), AlH_4NF_4(id: 696815*)
136	GeO_2(id: 470), SnO_2(id: 856), ZnF_2(id: 1873), TiO_2(id: 2657), MgH_2(id: 23710), KrF_2(id: 558928*), $CaBr_2$ (id: 571166*), HfO_2(id: 776532), $PbBr_2$(id: 862868*), $PbCl_2$(id: 862871*), YbO_2(id: 864801*), $YbCl_2$(id: 865716*),

TABLE III. (*Continued.*)

SG numbers	Materials
	YbF_2(id: 865934*), $TeBr_2$(id: 867355*), HgF_2(id: 974603*), SnI_2(id: 978846*), $SnBr_2$(id: 978985*), Li_2TiF_6(id: 7603), Li_2GeF_6(id: 7791), Na_2SnF_6(id: 8081), $MgTa_2O_6$(id: 9650), Li_2PdF_6(id: 13985), Li_2PtF_6(id: 13986), Ga_2TeO_6 (id: 28931), Tm_2TeO_6(id: 756339*), Lu_2TeO_6(id: 756389), $Zn(SbO_3)_2$(id: 3188), $Mg(SbO_3)_2$(id: 3653), $Ca_{11}(CN_5)_2$ (id: 4800*), $Na_2ZnP_2O_7$(id: 6491*), Li_3AuO_3(id: 7471*), BeO(id: 7599), Li_3BN_2(id: 8926*), $U(RhO_3)_2$(id: 13836), $K_2Na_4Be_2O_5$(id: 14324), $K_2ZnP_2O_7$(id: 16695), $TbCl_3$(id: 570232*), Li_3CuO_3(id: 19970*), Na_3AuO_2(id: 28365), $TlCu_5Se_3$(id: 541923), $Cs_2K_2TeO_5$(id: 556400*), Li_3BiO_4(id: 557738*), Ga_3Os(id: 570844), Rb_2H_4Pt(id: 642735), Cs_2H_4Pt(id: 643010), K_2H_4Pt(id: 974713), $RbLiZn_2O_3$(id: 18422), $KNiPS_4$(id: 662530), Na_3H_7Ru(id: 698032), Na_3CuO_2(id: 755401), Na_3CuO_3(id: 761827*), Na_3AuO_3(id: 768915*), $KPPdS_4$(id: 866637), Na_3H_7Os(id: 867943), $LiCa_{10}MgSb_9$(id: 569282), Rb_2H_4Pd(id: 644494)
137	ZrO_2(id: 2574), $Li_{10}Zn_4O_9$(id: 3297), Li_6WN_4(id: 3503), Li_6MoN_4(id: 8804), Li_6ZnO_4(id: 14495), Pb_2OF_2(id: 27355), Li_5TlO_4(id: 27483*), Cd_4OF_6(id: 28855), $K_4U(PO_5)_2$(id: 559639), $ZnCl_2$(id: 567279), HgI_2(id: 568742), Li_7VN_4 (id: 582259), $MgH_{12}(ClO_5)_2$(id: 707373*), Sn_2OF_2(id: 753683*), Ba_4OF_6(id: 754354), Na_6MgO_4(id: 755084), $BaNa_6O_4$ (id: 755322*), $MgP_2(H_8O_5)_2$(id: 758660*), Li_5BiO_4(id: 768986*), Na_5LaO_4(id: 780218*), Li_5LaO_4(id: 780259*), $CsGaH_4$(id: 984550*)
138	Sr_2SnO_4(id: 4287), $ZnPb_2F_6$(id: 20006*), $Hf(Se_2Cl_3)_2$(id: 29420*), SiO_2(id: 600109*), $Zr(Se_2Cl_3)_2$(id: 619928*), Sr_2HfO_4(id: 754761)

that 622 of them have two-NS phonons. However, the material candidates with SG Nos. 90 and 94 are missing in the phonon database. Based on the first-principles calculations and proposed symmetry conditions, we proposed 19 realistic materials, including $ZnTeMoO_6$, Cs_2Te_2, Sr_2SnO_4, CaAlPd, PtO_2, KLi_2As, CV_2, $BaVCu_4P_4O_{17}$, $Na_5Fe_3F_{14}$, BaS_3, Na_4SnS_4, ReO_3, $Sr_4Li_2Si_4N_8O$, $BaHfN_2$, Bi_2CuO_4, YB_2C, MgF_2, YB_4Rh_4, and $LiClO_2$, as materials with two-NS phonons. We believe that this paper can be viewed as a guide for further research into two-NS phonons. We also hope that this paper can be used for investigating the NS states in other bosonic systems, such as photon or magnon systems.

ACKNOWLEDGMENTS

Y.L. was grateful for support from the Nature Science Foundation of Hebei Province (Grant No. A2021202002). X.W. and H.Y. were grateful for support from the National Natural Science Foundation of China (Grants No. 51801163 and No. 11874306).

APPENDIX A: THE THEORETICAL AND EXPERIMENTAL LATTICE CONSTANTS FOR A SERIES OF SELECTED REALISTIC MATERIALS WITH TWO-NS PHONONS

We exhibited the theoretical and experimental lattice constants for a series of selected realistic materials with two-NS phonons (see Table II). Obviously, the theoretical lattice constants and the experimental lattice constants for these nineteen materials are in good agreement as listed in Table II.

APPENDIX B: SELECTED MATERIALS WITH TWO-NS PHONONS IN THE PHONON DATABASE AT KYOTO UNIVERSITY

To support the inspirational findings of two-NS phonons, we discovered that 622 of 10037 materials listed in the phonon database at Kyoto University have two-NS phonons. A list of these 622 materials as well as their SG numbers and materials'ids are shown in Table III.

[1] Z.-M. Yu, Z. Zhang, G.-B. Liu, W. Wu, X.-P. Li, R.-W. Zhang, S. A. Yang, and Y. Yao, Sci. Bull. **67**, 375 (2022).
[2] G.-B. Liu, Z. Zhang, Z.-M. Yu, S. A. Yang, and Y. Yao, arXiv:2111.04372.
[3] N. Nagaosa, T. Morimoto, and Y. Tokura, Nat. Rev. Mater. **5**, 621 (2020).
[4] B. Yan and C. Felser, Annu. Rev. Condens. Matter Phys. **8**, 337 (2017).
[5] S. A. Yang, SPIN **06**, 1640003 (2016).
[6] T. O. Wehling, A. M. Black-Schaffer, and A. V. Balatsky, Adv. Phys. **63**, 1 (2014).
[7] C. W. J. Beenakker, Annu. Rev. Condens. Matter Phys. **4**, 113 (2013).
[8] A. Y. Kitaev, Phys.-Usp. **44**, 131 (2001).
[9] P. Li, Y. Wen, X. He, Q. Zhang, C. Xia, Z.-M. Yu, S. A. Yang, Z. Zhu, H. N. Alshareef, and X.-X. Zhang, Nat. Commun. **8**, 2150 (2017).
[10] S. Guan, Z.-M. Yu, Y. Liu, G.-B. Liu, L. Dong, Y. Lu, Y. Yao, and S. A. Yang, npj Quantum Mater. **2**, 23 (2017).
[11] A. Bernevig, H. Weng, Z. Fang, and X. Dai, J. Phys. Soc. Jpn. **87**, 041001 (2018).
[12] S.-Y. Yang, H. Yang, E. Derunova, S. S. P. Parkin, B. Yan, and M. N. Ali, Adv. Phys. X **3**, 1414631 (2018).
[13] R. Yu, Z. Fang, X. Dai, and H. Weng, Front. Phys. **12**, 127202 (2017).
[14] C. Fang, Y. Chen, H.-Y. Kee, and L. Fu, Phys. Rev. B **92**, 081201(R) (2015).
[15] A. A. Soluyanov, D. Gresch, Z. Wang, Q. Wu, M. Troyer, X. Dai, and B. A. Bernevig, Nature (London) **527**, 495 (2015).
[16] M. Vergniory, L. Elcoro, C. Felser, N. Regnault, B. A. Bernevig, and Z. Wang, Nature (London) **566**, 480 (2019).
[17] F. Tang, H. C. Po, A. Vishwanath, and X. Wan, Nature (London) **566**, 486 (2019).

[18] S. M. Young and C. L. Kane, Phys. Rev. Lett. **115**, 126803 (2015).
[19] B.-J. Yang and N. Nagaosa, Nat. Commun. **5**, 4898 (2014).
[20] B. J. Wieder, Y. Kim, A. M. Rappe, and C. L. Kane, Phys. Rev. Lett. **116**, 186402 (2016).
[21] Q. D. Gibson, L. M. Schoop, L. Muechler, L. S. Xie, M. Hirschberger, N. P. Ong, R. Car, and R. J. Cava, Phys. Rev. B **91**, 205128 (2015).
[22] T.-R. Chang, S.-Y. Xu, D. S. Sanchez, W.-F. Tsai, S.-M. Huang, G. Chang, C.-H. Hsu, G. Bian, I. Belopolski, Z.-M. Yu, S. A. Yang, T. Neupert, H.-T. Jeng, H. Lin, and M. Z. Hasan, Phys. Rev. Lett. **119**, 026404 (2017).
[23] Z. Zhu, Z.-M. Yu, W. Wu, L. Zhang, W. Zhang, F. Zhang, and S. A. Yang, Phys. Rev. B **100**, 161401(R) (2019).
[24] K.-H. Ahn, W. E. Pickett, and K.-W. Lee, Phys. Rev. B **98**, 035130 (2018).
[25] Z. P. Sun, C. Q. Hua, X. L. Liu, Z. T. Liu, M. Ye, S. Qiao, Z. H. Liu, J. S. Liu, Y. F. Guo, Y. H. Lu, and D. W. Shen, Phys. Rev. B **101**, 155114 (2020).
[26] D.-S. Ma, J. Zhou, B. Fu, Z.-M. Yu, C.-C. Liu, and Y. Yao, Phys. Rev. B **98**, 201104(R) (2018).
[27] X.-P. Li, B. Fu, D.-S. Ma, C. Cui, Z.-M. Yu, and Y. Yao, Phys. Rev. B **103**, L161109 (2021).
[28] Z. Zhang, Z.-M. Yu, and S. A. Yang, Phys. Rev. B **103**, 115112 (2021).
[29] S. Li, Y. Liu, S.-S. Wang, Z.-M. Yu, S. Guan, X.-L. Sheng, Y. Yao, and S. A. Yang, Phys. Rev. B **97**, 045131 (2018).
[30] X.-L. Sheng, Z.-M. Yu, R. Yu, H. Weng, and S. A. Yang, J. Phys. Chem. Lett. **8**, 3506 (2017).
[31] W. Wu, Y. Liu, S. Li, C. Zhong, Z.-M. Yu, X.-L. Sheng, Y. X. Zhao, and S. A. Yang, Phys. Rev. B **97**, 115125 (2018).
[32] X. M. Zhang, Z.-M. Yu, Z. M. Zhu, W. K. Wu, S.-S. Wang, X.-L. Sheng, and S. A. Yang, Phys. Rev. B **97**, 235150 (2018).
[33] Q.-F. Liang, J. Zhou, R. Yu, Z. Wang, and H. Weng, Phys. Rev. B **93**, 085427 (2016).
[34] A. Topp, R. Queiroz, A. Grüneis, L. Müchler, A. W. Rost, A. Varykhalov, D. Marchenko, M. Krivenkov, F. Rodolakis, J. L. McChesney, B. V. Lotsch, L. M. Schoop, and C. R. Ast, Phys. Rev. X **7**, 041073 (2017).
[35] C. Chen, X. Xu, J. Jiang, S.-C. Wu, Y. P. Qi, L. X. Yang, M. X. Wang, Y. Sun, N. B. M. Schröter, H. F. Yang, L. M. Schoop, Y. Y. Lv, J. Zhou, Y. B. Chen, S. H. Yao, M. H. Lu, Y. F. Chen, C. Felser, B. H. Yan, Z. K. Liu, and Y. L. Chen, Phys. Rev. B **95**, 125126 (2017).
[36] X. Chen, J. Liu, and J. Li, Innovation **2**, 100134 (2021).
[37] J. Li, J. Liu, S. A. Baronett, M. Liu, L. Wang, R. Li, Y. Chen, D. Li, Q. Zhu, and X.-Q. Chen, Nat. Commun. **12**, 1204 (2021).
[38] G. Liu, Y. Jin, Z. Chen, and H. Xu, Phys. Rev. B **104**, 024304 (2021).
[39] J.-Y. You, X.-L. Sheng, and G. Su, Phys. Rev. B **103**, 165143 (2021).
[40] F. Zhou, Z. Zhang, H. Chen, M. Kuang, T. Yang, and X. Wang, Phys. Rev. B **104**, 174108 (2021).
[41] J. Zhu, W. Wu, J. Zhao, H. Chen, L. Zhang, and S. A. Yang, arXiv:2104.14816.
[42] F. Zhou, H. Chen, Z.-M. Yu, Z. Zhang, and X. Wang, Phys. Rev. B **104**, 214310 (2021).
[43] Y. S. Chen, F. F. Huang, P. Zhou, Z. S. Ma, and L. Z. Sun, New J. Phys. **23**, 103043 (2021).
[44] Q.-B. Liu, H.-H. Fu, and R. Q. Wu, Phys. Rev. B **104**, 045409 (2021).
[45] Q.-B. Liu, Z. Wang, and H.-H. Fu, Phys. Rev. B **103**, L161303 (2021).
[46] Q.-B. Liu, Y. Qian, H.-H. Fu, and Z. Wang, npj Comput. Mater. **6**, 95 (2020).
[47] J. Wang, H. Yuan, Z.-M. Yu, Z. Zhang, and X. Wang, Phys. Rev. Mater. **5**, 124203 (2021).
[48] T. T. Zhang, Z. D. Song, A. Alexandradinata, H. M. Weng, C. Fang, L. Lu, and Z. Fang, Phys. Rev. Lett. **120**, 016401 (2018).
[49] H. Miao, T. T. Zhang, L. Wang, D. Meyers, A. H. Said, Y. L. Wang, Y. G. Shi, H. M. Weng, Z. Fang, and M. P. M. Dean, Phys. Rev. Lett. **121**, 035302 (2018).
[50] Y. J. Jin, Z. J. Chen, X. L. Xiao, and H. Xu, Phys. Rev. B **103**, 104101 (2021).
[51] Z. Huang, Z. Chen, B. Zheng, and H. Xu, npj Comput. Mater. **6**, 87 (2020).
[52] R. Wang, B. W. Xia, Z. J. Chen, B. B. Zheng, Y. J. Zhao, and H. Xu, Phys. Rev. Lett. **124**, 105303 (2020).
[53] S. Singh, Q. S. Wu, C. M. Yue, A. H. Romero, and A. A. Soluyanov, Phys. Rev. Mater. **2**, 114204 (2018).
[54] C. Xie, Y. Liu, Z. Zhang, F. Zhou, T. Yang, M. Kuang, X. Wang, and G. Zhang, Phys. Rev. B **104**, 045148 (2021).
[55] Q.-B. Liu, Z.-Q. Wang, and H.-H. Fu, Phys. Rev. B **104**, L041405 (2021).
[56] M. Zhong, Y. Liu, F. Zhou, M. Kuang, T. Yang, X. Wang, and G. Zhang, Phys. Rev. B **104**, 085118 (2021).
[57] C. W. Xie, H. K. Yuan, Y. Liu, X. T. Wang, and G. Zhang, Phys. Rev. B **104**, 134303 (2021).
[58] J. Wang, H. Yuan, M. Kuang, T. Yang, Z.-M. Yu, Z. Zhang, and X. Wang, Phys. Rev. B **104**, L041107 (2021).
[59] Z.-M. Yu, W. Wu, Y. X. Zhao, and S. A. Yang, Phys. Rev. B **100**, 041118(R) (2019).
[60] X. Wang, F. Zhou, T. Yang, M. Kuang, Z.-M. Yu, and G. Zhang, Phys. Rev. B **104**, L041104 (2021).
[61] http://phonondb.mtl.kyoto-u.ac.jp/.
[62] See Supplemental Material at http://link.aps.org/supplemental/10.1103/PhysRevB.105.054307 for the computational methods, crystal structures, and calculated phonon dispersions for 11 materials with two-NS phonons.
[63] G. Kresse and J. Furthmuller, Phys. Rev. B **54**, 11169 (1996).
[64] J. P. Perdew, K. Burke, and M. Ernzerhof, Phys. Rev. Lett. **77**, 3865 (1996).
[65] https://github.com/quanshengwu/wanniertools/tree/master/utility/phonopyTB.
[66] Q. Wu, S. Zhang, H. Song, M. Troyer, and A. Soluyanov, Comput. Phys. Commun. **224**, 405 (2018).
[67] F. Guinea, C. Tejedor, F. Flores, and E. Louis, Phys. Rev. B **28**, 4397 (1983).
[68] J. W. Hobbs and R. J. Pulham, J. Chem. Res. (S) **4**, 156 (1994).
[69] Y. Doi, R. Suzuki, Y. Hinatsu, and K. Ohoyama, J. Phys.: Condens. Matter **21**, 046006 (2009).
[70] H. Zhu, M. Q. Zhang, B. Li, Y. Y. Liu, J. Zhuang, X. Y. Zhao, M. Xue, L. Wang, Y. Liu, and X. T. Tao, J. Super. Fluids **171**, 105187 (2021).
[71] W. T. Fu and D. Visser, and D. J. W. IJdo, J. Solid State Chem. **169**, 208 (2002).
[72] G. Cordier and T. Friedrich, Z. Kristallogr. **205**, 135 (1993).
[73] O. Muller and R. Roy, J. Less-Common Met. **16**, 129 (1968).

[74] R. H. C. Gil, W. Hönle, and H.-G. V. Schnering, Z. Anorg. Allg. Chem. **622**, 319 (1996).
[75] K. Yvon, W. Rieger, and H. Nowotny, Monatsh. Chem. **97**, 689 (1966).
[76] H.-G. V. Schnering and N. K. Goh, Naturwiss. **61**, 272 (1974).
[77] S. Meyer and H. Müller-Buschbaum, Z. Anorg. Allg. Chem. **623**, 1693 (1997).
[78] M. Vlasse, F. Menil, C. Moriliere, J. M. Dance, A. Tressaud, and J. Portier, J. Solid State Chem. **17**, 291 (1976).
[79] J. C. Jumas, E. Philippot, F. Vermot-Gaud-Daniel, M. Ribes, and M. Maurin, J. Solid State Chem. **14**, 319 (1975).
[80] J.-E. Jorgensen, J. D. Jorgensen, B. Batlogg, J. P. Remeika, and J. D. Axe, Phys. Rev. B **33**, 4793 (1986).
[81] S. Pagano, S. Lupart, M. Zeuner, and W. Schnick, Angew. Chem. **121**, 6453 (2009).
[82] D. H. Gregory, M. G. Barker, P. P. Edwards, M. Slaski, and D. J. Siddons, J. Solid State Chem. **137**, 62 (1998).
[83] M. T. Weller and D. R. Lines, J. Solid State Chem. **82**, 21 (1989).
[84] J. Bauer and J. Debuigne, J. Inorg. Nucl. Chem. **37**, 2473 (1975).
[85] W. H. Baur, Acta Cryst. **9**, 515 (1956).
[86] J. M. Vandenberg and B. T. Matthias, Proc. Natl. Acad. Sci. USA **74**, 1336 (1977).
[87] A. I. Smolentsev and D. Y. Naumov, Acta Cryst. C **61**, i17 (2005).